# Spoof plasmon polaritons in slanted geometries

J. J. Wood, L. A. Tomlinson, O. Hess, S. A. Maier, and A. I. Fernández-Domínguez
*The Blackett Laboratory, Department of Physics, Imperial College London, London SW7 2AZ, UK*
(Received 19 December 2011; published 29 February 2012)

We present a refined quasianalytical approach that provides a complete description of the modal characteristics of the spoof plasmon modes sustained by a periodic array of slanted grooves. Specifically, our method yields deep physical insight into the effect that the orientation of the supporting structure has on the dispersion properties and field confinement capabilities of these geometrically induced surface electromagnetic waves.

DOI: 10.1103/PhysRevB.85.075441 PACS number(s): 42.79.Gn, 73.20.Mf, 42.79.Dj, 78.68.+m

## I. INTRODUCTION

The remarkable ability of surface plasmon polaritons[1] (SPPs)—electromagnetic (EM) surface waves sustained at the interface between a conductor and a dielectric—to guide and localize light into the subwavelength scale has attracted a great deal of attention during the last decade.[2] Moreover, the recent development of powerful nanofabrication and characterization techniques has promoted a deep exploration of the technological capabilities of these confined EM waves in areas such as optoelectronics, materials science, and biosensing.[3–5] Although most plasmonic research so far has focused on the near-infrared and optical ranges of the EM spectrum (where noble metals support highly confined surface waves), there exists increasing interest in transferring SPP-based photonics to lower frequencies, such as microwave or terahertz (THz). However, in these spectral ranges, noble metals behave like perfect electric conductors (PECs), whose surface charges are able to screen any external EM excitation with extreme efficiency, preventing the formation of tightly bound SPPs.

Since the middle of the last century, it has been well-known that the binding of EM fields to a metal surface can be increased by its corrugation.[6–8] However, it was not until 2004 when the strategy to reproduce the modal characteristics of plasmonic modes at low-frequency domains was clarified. Using an elegant metamaterial approach, Pendry and coworkers[9] demonstrated that confined EM waves mimicking SPPs can be created at the surface of a PEC through its subwavelength structuring. This led to the spoof plasmon concept, which was subsequently verified experimentally at microwave[10] and THz frequencies.[11] Importantly, although the first studies analyzing spoof SPPs considered simple planar geometries,[12–20] lately more complex waveguiding schemes exploiting these surface EM modes have been proposed theoretically[21–26] and realized experimentally.[27–37] All these designs feature deep subwavelength transverse confinement of microwave or THz waves while keeping long propagation distances, modal characteristics which are unattainable otherwise. More recently, the spoof plasmon concept has been proposed as a means to achieve broadband transparency,[38] directional beaming,[39] and nonreciprocal transmission[40] of EM radiation.

Contrary to conventional SPPs, whose attributes are dictated by the intrinsic dielectric properties of their supporting material, spoof plasmon modes are entirely governed by the geometry of the corrugated surface sustaining them, provided the surface acts as a perfect conductor. Thus, the geometrically induced nature of spoof SPPs translates into the possibility of tailoring their properties through design. Although a wide range of spoof plasmon waveguides have been developed so far, most research efforts have explored the dependence of their performance on the dimensions of the indentations decorating them. In this paper, we introduce a new degree of freedom in these designs by investigating theoretically how the orientation of the surface structuring modifies the dispersion and field confinement capabilities of spoof SPPs. Specifically, we present an insightful modal expansion formalism that enables us to analyze the spoof plasmon modes sustained by a periodic array of slanted grooves, the simplest geometry where orientation effects come into play. Note that although slanted gratings have been extensively used in conventional waveguide coupling[41–44] and SPP excitation,[45] their spoof plasmon guiding capabilities have not yet been investigated. Our approach yields approximate analytic expressions for the spoof SPP dispersion relation and associated EM fields, which gives a deep physical insight into their dependence on the angle of orientation of the grooves. Finally, we extend our method to sawtooth and triangular indentations, showing the validity of our theoretical results for these geometries through the comparison with full field numerical calculations.

## II. THEORETICAL APPROACH

Figure 1 depicts the structure under consideration. It is a PEC block whose surface is perforated with a periodic arrangement of slanted grooves. Four parameters characterize the geometry: the array pitch $d$, the width $a$, and the height $h$ of the grooves, and their orientation angle $\theta$. Note that $a$ ($h$) is defined at the groove's bottom (center plane), and that $\theta$ is measured from the surface normal. Moreover, as the structure is perfectly conducting, all the lengths in the system are scalable and we can take the period $d$ as the reference length. We have developed a theoretical approach to investigate the spoof SPP modes supported by this structure. Our method is based on the modal expansion technique,[46] which has been exploited in the study of spoof plasmons in straight geometries,[47] as well as in other fields of research such as double fishnet metamaterials[48] or the extraordinary transmission phenomenon.[49]

We divide the geometry in Fig. 1 into two different regions and express the EM fields in each of them in terms of the most convenient set of solutions of Maxwell's equations. Note that the structure presents translational symmetry along the $y$ direction, parallel to the grooves. This allows us to restrict our analysis to the perpendicular plane where light polarizations

 

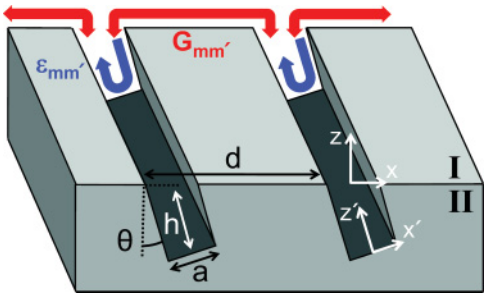


FIG. 1. (Color online) Schematic view of the most general geometry analyzed in this paper: a periodic array of slanted grooves perforated in a PEC surface. The parameters defining the structure are the array pitch $d$, the groove width $a$, the groove height $h$, and the slant angle $\theta$. The physical interpretation of the various terms in Eq. (5), which expresses the continuity of the EM fields at the interface between regions I and II, is also sketched.

are decoupled, and consider only $p$-polarized fields, which are fully described through the $y$ component of the magnetic field (the only nonzero), $H_y$. The electric field components can be straightforwardly obtained by applying the Maxwell curl equations on $H_y$. Taking advantage of the periodic character of the system, we restrict our analysis to a single unit cell of length $d$. Thus, in region I, which corresponds to the free space above the PEC structure, $H_y$ can be expanded into diffracted plane waves, having

$$H_y^I(x,z) = \sum_{n=-\infty}^{\infty} r_n Y_n^I e^{-q_n^I z}\phi_n(x), \tag{1}$$

where $\phi_n(x) = e^{ik_n x}/\sqrt{d}$ is the $n$th diffraction order wave function, $k_n = k_x + n\frac{2\pi}{d}$ and $q_n^I = \sqrt{k_n^2 - k_\omega^2}$ are its wave-vector components, and $Y_n^I = -ik_\omega/q_n^I$ is the modal admittance. Note that we have introduced the free-space wave-vector modulus $k_\omega = \omega/c = 2\pi/\lambda$, and set the zero-order parallel wave vector $k_0 = k_x$. Equation (1) is evaluated using the unprimed coordinates $(x,z)$, defined as indicated in Fig. 1.

Region II ranges over both the PEC block, where both the electric and magnetic fields vanish, and the surface indentations, where EM fields can be expressed in terms of groove waveguide modes. These must be evaluated using the prime coordinates $(x',z')$, whose origin is located at the center of the groove bottom and are slanted at an angle $\theta$ with respect to the unprimed ones (see Fig. 1). The primed and unprimed coordinates can be related simply to one another by $x' = \cos\theta x + \sin\theta z$, $y' = y$, and $z' = h - \sin\theta x + \cos\theta z$. In terms of the primed coordinates, the $y'$ component of the magnetic field within the groove reads

$$H_{y'}^{II}(x',z') = \sum_{m=0}^{\infty} Y_m^{II} A_m \cos\left(q_m^{II} z'\right)\chi_m(x'), \tag{2}$$

where $\chi_m(x') = \sqrt{(2-\delta_{m0})/a}\cos[\frac{m\pi}{a}(x'+\frac{a}{2})]$ is the wave function for the $m$th guided mode.[50] The corresponding normal wave vector and modal admittance are $q_m^{II} = \sqrt{k_\omega^2 - (m\pi/a)^2}$ and $Y_m^{II} = -ik_\omega/q_m^{II}$, respectively.

As a result of the modal expansion procedure, the only unknowns of the system are the set of coefficients $\{r_n, A_m\}$. These are the only ingredients needed to construct the EM fields in both regions. They can be calculated by imposing continuity conditions on the fields at the interface between regions I and II ($z = 0$). At this boundary, the $x$ component of the electric field must be continuous across the whole interface, whereas the $y$ component of the magnetic field is only continuous at the groove's opening. In order to perform the field matching, $E_x^{II}(x,z=0)$ (in the unprimed frame) must be calculated from the primed electric field components. Thus, the two continuity conditions can be written as

$$E_x^I(x,0) = \cos\theta E_{x'}^{II}(\cos\theta x, h - \sin\theta x) - \sin\theta E_{z'}^{II}(\cos\theta x, h - \sin\theta x), \tag{3}$$

$$H_y^I(x,0) = H_{y'}^{II}(\cos\theta x, h - \sin\theta x). \tag{4}$$

In order to remove the $x$ dependence of these equations, we project Eq. (3) into diffracted plane waves, $\phi_n(x)$, and Eq. (4) into groove wave-guide modes, $\chi_m(\cos\theta x)$. The resulting algebraic equations can then be combined and rewritten as a set of $m \times m$ system of equations of the form

$$\sum_{m'}(G_{mm'} - \epsilon_{mm'})E_{m'} = 0, \tag{5}$$

where the unknowns, $E_m = A_m \sin(q_m^{II} h)$, are linked to the expansion coefficients in Eq. (2), and can be interpreted as the $m$-modal amplitude of $E_x$ at $z = 0$.[49] The term

$$\epsilon_{mm'} = \frac{Y_{m'}^{II}}{\sin\left(q_{m'}^{II} h\right)} \int_{-a/2\cos\theta}^{a/2\cos\theta} \chi_m^*(\cos\theta x)\cos\left[q_{m'}^{II}(h - \sin\theta x)\right] \times \chi_{m'}(\cos\theta x)\,\cos\theta\,dx \tag{6}$$

describes the bouncing back and forth of the $m'$th waveguide mode inside the indentations and its coupling to $\chi_m(x)$ (with $m \neq m'$ in general) at the groove opening. For $\theta = 0°$, Eq. (6) gives $\epsilon_{mm'} = Y_{m'}^{II}\cot(q_{m'}^{II} h)\delta_{mm'}$. This recovers the result for straight geometries, in which the reflection of the groove waveguide modes at the system interface does not lead to the overlapping among EM fields associated with different $m$'s.[47]

The term $G_{mm'}$ in Eq. (5) reflects the EM coupling between $m$ and $m'$ groove waveguide modes through diffracted waves. It takes into account the radiation emitted by $\chi_{m'}(x\cos\theta)$ into free space, and its collection back at the structure indentations by $\chi_m(x\cos\theta)$. It has the form

$$G_{mm'} = \sum_n Y_n^I S_{mn}[\cos\theta X_{nm'} - \sin\theta Z_{nm'}], \tag{7}$$

where

$$S_{mn} = \int_{-a/2\cos\theta}^{a/2\cos\theta} \chi_m^*(x\cos\theta)\phi_n(x)\,\cos\theta\,dx \tag{8}$$

gives the overlapping between diffracted waves and waveguide modes at the groove opening. Equation (7) describes the EM interaction among the fields at different indentations. The physical interpretation of $G_{mm'}$ and $\epsilon_{mm'}$ is sketched in Fig. 1. The elements

$$X_{nm'} = \frac{1}{\sin\left(q_{m'}^{II} h\right)} \int_{-a/2\cos\theta}^{a/2\cos\theta} \phi_n^*(x)\sin\left[q_{m'}^{II}(h - \sin\theta x)\right] \times \chi_{m'}(\cos\theta x)\,dx, \tag{9}$$

$$Z_{nm'} = \frac{-im'\pi Y^{II}_{m'}}{ak_\omega \sin\left(q^{II}_{m'}h\right)} \int_{-a/2\cos\theta}^{a/2\cos\theta} \phi^*_n(x)\cos\left[q^{II}_{m'}(h-\sin\theta x)\right] \times \tan\left[\frac{m'\pi}{a}\left(\cos\theta x+\frac{a}{2}\right)\right]\chi_{m'}(\cos\theta x)\,dx, \quad (10)$$

weight the contributions of $E^{II}_{x'}$ and $E^{II}_{z'}$ to Eq. (4), respectively. At $\theta = 0^\circ$, both coordinate systems are parallel and the continuity equation reads $E^{II}_{x'} = E^{II}_{x}$. In this limit, $X_{nm'} = S^*_{m'n}$ and Eq. (7) yields $G_{mm'} = \sum_n Y^I_n S_{mn} S^*_{m'n}$. This reproduces the result for straight corrugations. Let us stress that all the overlap integrals above can be calculated analytically (see Appendix), hence forming a closed and elegant theoretical description of the system.

The spoof SPP modes supported by the structure shown in Fig. 1 correspond to the nontrivial ($E_m \neq 0$) solutions of Eq. (5). Specifically, the spoof plasmon dispersion relation is given by the values of the parallel wave vector $k_x$ and frequency $\omega$, which produce a vanishing determinant associated with these continuity equations. In general, this problem must be solved numerically by scanning over $k_\omega$ and $k_x$ and searching for zeros in the determinant associated with Eqs. (5). However, an analytical expression for $\omega = \omega(k_x)$ can be obtained under two assumptions.[49] First, for deeply subwavelength indentations ($\lambda \gg a$), only the lowest waveguide mode is propagating inside the grooves. This allows us to restrict the sum in Eq. (4) to the $m = 0$ term, as it governs the EM fields behavior inside the indentations. Note that this assumption is more restrictive in slanted geometries than in the straight case, as it disregards the EM coupling among different waveguide modes described by Eq. (6). Second, in the limit of wavelengths much larger than the structure period ($\lambda \gg d$), diffraction effects can be neglected and we can keep only the $n = 0$ order in Eq. (3). This is equivalent to describing the array of indentations as a metamaterial structure characterized by a homogeneous permittivity and permeability.

Under the two assumptions discussed above, the dispersion relation for the spoof SPPs in slanted geometries can be written in the same form as for straight indentations:[12]

$$k_x(\omega) = k_\omega\sqrt{1+\left(\frac{a_{\rm eff}(k_\omega,\theta)}{d}\right)^2\tan^2(k_\omega h)}, \quad (11)$$

where we have introduced an effective groove width $a_{\rm eff}(k_\omega,\theta) = a\,\mathrm{sinc}^{-1}[(k_\omega a/2)\tan\theta] \simeq a[1+(\pi^2/6)(a\tan\theta/\lambda)^2]$. The transformation of Eqs. (5) to (11) is shown in the Appendix. According to Eq. (11), the spoof SPP asymptotic behavior ($k_x \to \infty$) is not affected by the rotation of the indentations. This indicates that it is the actual dimension of the grooves, $h$, and not their depth along the direction normal to the PEC surface, $h\cos\theta$, which controls the spoof SPP characteristics.

Equation (11) predicts an effective widening of the indentations with the slant angle through $a_{\rm eff}(k_\omega,\theta)$. This enlargement does not only reflect the fact that the slanted grooves are wider at their opening than at their bottom, $a/\cos\theta > a$, but also the sensitivity of the spoof SPP fields to the groove dimensions. It is important to note that although $\omega(k_x \to \infty)$ is unaffected by the rotation of the groove, the associated widening of the slit increases the slope with which the spoof SPP band approaches this asymptote. This alters the curvature of the dispersion relation and makes the frequency at the edge of the first Brillouin zone ($k_x = \pi/d$) dependent on $\theta$. Let us stress that despite its approximate character, Eq. (11) provides physical insight into the dependence of the spoof SPP characteristics on the various geometric parameters defining the structure in Fig. 1.

## III. RESULTS AND DISCUSSION

Figure 2 plots the dispersion relation of the spoof plasmon modes supported by a periodic array of grooves of width $a = 0.4d$ and height $h = 0.4d$, and three different orientations $\theta$: 10° (blue), 30° (green), and 45° (red). Note that only confined bands are rendered, while the leaky region above the light line is shaded in gray. The spoof SPP bands were calculated including as many diffraction orders ($n_{\max} = 10$) and waveguide modes ($m_{\max} = 2$) as needed to reach convergence in the solution of Eq. (5). The main panel of Fig. 2 shows that by slanting the grooves, the spoof plasmon dispersion relation shifts to higher frequencies. This trend is predicted by Eq. (11), where the effective widening of the indentation's size with $\theta$ leads to a faster growth of the modal frequency with increasing parallel wave vector. Let us stress that the 10° band virtually overlaps with the one for straight grooves (not shown). This observation is also in good agreement with our approximate expression for $a_{\rm eff}(k_\omega,\theta)$, which for the geometric parameters considered yields an effective enlargement of only 5% in the groove's width at the spoof SPP band edge ($k_x = \pi/d$).

The left (right) inset of Fig. 2 displays the normalized frequency, $d/\lambda$, evaluated at the spoof SPP band edge as a function of the slant angle and the groove's width (height) for $h = 0.4d$ ($a = 0.4d$). In both panels, colors render $d/\lambda$ in a linear scale from 0.15 (blue) to 0.43 (red). For all the groove dimensions considered, increasing the slant angle blueshifts the normalized frequency and moves the spoof plasmon bands closer to the light line. As stated previously, this originates

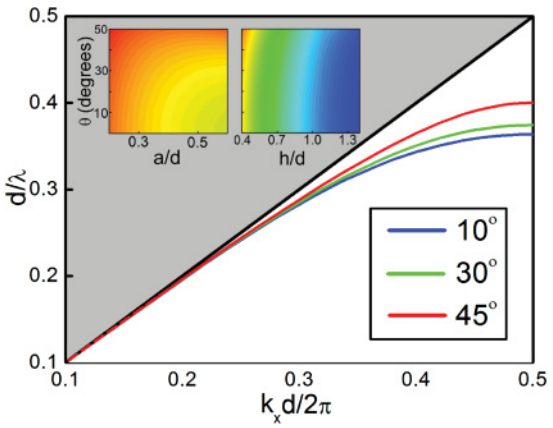


FIG. 2. (Color online) Spoof SPP dispersion relation for an array of grooves of dimensions $a = 0.4d$ and $h = 0.4d$, and three different orientation angles $\theta$. The black line plots the light line, $k_\omega = k_x$. Left inset: Normalized spoof SPP frequency, $d/\lambda$, evaluated at the band edge ($k_x = \pi/d$) as a function of the slant angle and the groove width for $h = 0.4d$. Right inset: The same as before but as a function of the groove height for $a = 0.4d$. In both insets the linear color scale ranges from 0.15 (blue) to 0.43 (red).

from the effective enlargement of the width of the indentations with $\theta$. The left inset of Fig. 2 indicates that this trend is more pronounced for wide grooves ($a \gtrsim 0.4d$) than for narrow ones, which can be explained in terms of $a_{\text{eff}}(k_\omega,\theta)$. $a_{\text{eff}}$ grows as the square of $a\tan\theta/\lambda$ and hence the spoof plasmon modes sustained by wide indentations are more sensitive to variations in their orientation. On the other hand, the right inset of Fig. 2 shows that deep grooves ($h \gtrsim d$) support spoof SPPs whose modal characteristics depend very weakly on $\theta$. This can be understood from Eq. (11), which, for large $h$, is governed by the $\tan(k_\omega h)$ divergent term. For shallower indentations, the competition between width and depth effects makes the spoof SPPs less robust to variations in the slant angle.

In order to test the validity of our theoretical approach and to investigate its convergence with the number of groove waveguide modes, $m_{\max}$, we compare our quasianalytical results with finite-element simulations. The commercial program COMSOL MULTIPHYSICS was used to calculate numerically the spoof SPP bands for different geometries, which were then contrasted to the solution of Eq. (5) for $m_{\max} = 0$, 1, and 2. In the upper panel of Fig. 3, this comparison is shown for indentations of dimension $a = 0.3d$ and $h = 0.5d$, and two different orientations, 10° (green line) and 45° (red line). For small $\theta$, the truncation of the sum in Eq. (2) modifies the spoof SPP dispersion relation by a very small amount, and considering only the lowest ($m = 0$) groove waveguide mode yields accurate results. On the other hand, for larger slant angles, more waveguide modes are required to reach convergence. This observation can be linked to the effective enlargement of the groove width with increasing $\theta$. Note that the validity of the $m = 0$ approximation lies in the fact that for narrow indentations, higher waveguide modes are evanescent. This assumption also fails when the grooves are highly slanted, as the complex field pattern at the indentation opening cannot be correctly described through the lowest waveguide mode. As predicted by Eq. (6), the field matching at the groove opening gives rise to the EM coupling among different waveguide modes. This effect is enhanced for large $\theta$, which also explains the failure of the $m = 0$ approximation. Despite these limitations, it is remarkable that as shown in the upper panel of Fig. 3, spoof SPP bands calculated with $m_{\max} = 2$ are in excellent agreement with numerical simulations.

The lower panels of Fig. 3 depict the $x$ component of the electric field evaluated at the edge of the first Brillouin zone for $a = 0.3d$ and $h = 0.5d$, and a range of orientation angles. All the field maps were calculated by considering only the lowest groove waveguide mode in the field expansion. As $\theta$ increases, the electric field pattern becomes more asymmetric at the groove opening. This effect is accompanied by the enlargement of the spread of the fields in region I, a consequence of the reduced confinement of the spoof SPP modes. Note that as a result of the blueshift experienced by the spoof SPP bands with increasing $\theta$, the fields in Fig. 3 corresponding to geometries with a greater slant angle are evaluated at higher frequencies. As a consequence of the $m = 0$ approximation, the fields inside the indentation remain very similar with increasing $\theta$, only undergoing a rotation. Moreover, $E_x$ becomes increasingly mismatched at the interface between regions I and II as $\theta$ increases, which is a clear indication of the failure of the

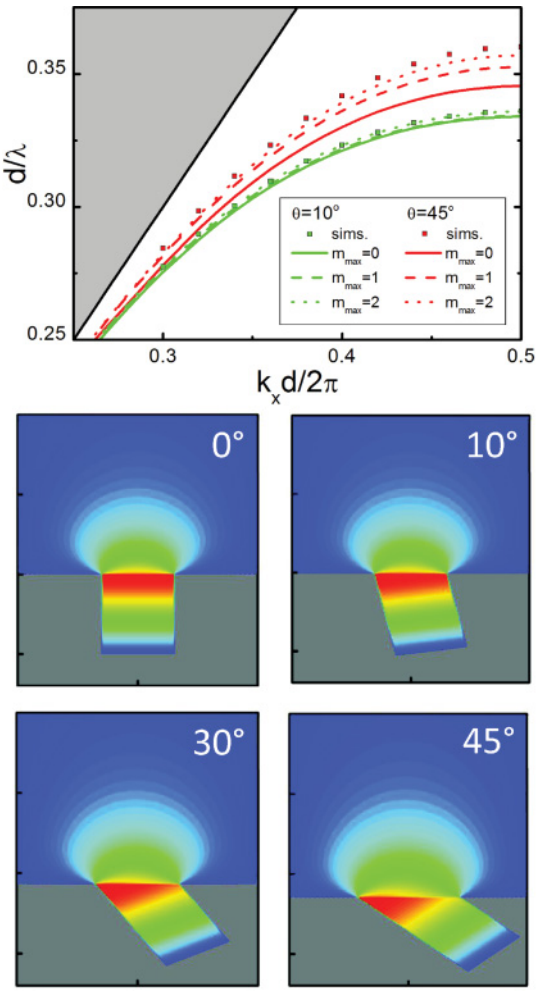


FIG. 3. (Color online) Upper panel: Spoof SPP dispersion relation for indentations with $a = 0.3d$, $h = 0.5d$, and two different slant angles: 10° (green) and 45° (red). Bands obtained considering one (solid line), two (dashed line), and three (dotted line) waveguide modes in Eq. (5) are plotted, together with simulations results (square dots). Lower panels: $E_x$ evaluated at $k_x = \pi/d$ for four different groove orientations. Fields were calculated using the single waveguide mode ($m_{\max} = 0$) approximation. In all cases the linear color scale ranges from blue (minimum) to red (maximum).

approximation at large slant angles. Note that the fields in Fig. 3 are evaluated at the band edge ($k_x = \pi/d$), which maximizes the field confinement and localization within the groove.

To further investigate spoof SPPs in slanted geometries, it is convenient to introduce a new parameter $b$. This is defined as the width of the groove at its opening, related to $a$ via $b = a/\cos\theta$. So far we have analyzed the effect of rotating a rectangular groove in a metal surface by an arbitrary $\theta$. As a variation of this geometry, it is possible to increase the slant angle until the shorter side of the groove vanishes. At this point, the indentation forms a triangular dent carved into the PEC surface. This structure is realizable provided $(2h)^2 + a^2 \leqslant d^2$, and the relation between the orientation angle $\theta$ and $a$ and $h$ reads

$$\theta = \arctan\left(\frac{2h}{a}\right). \tag{12}$$

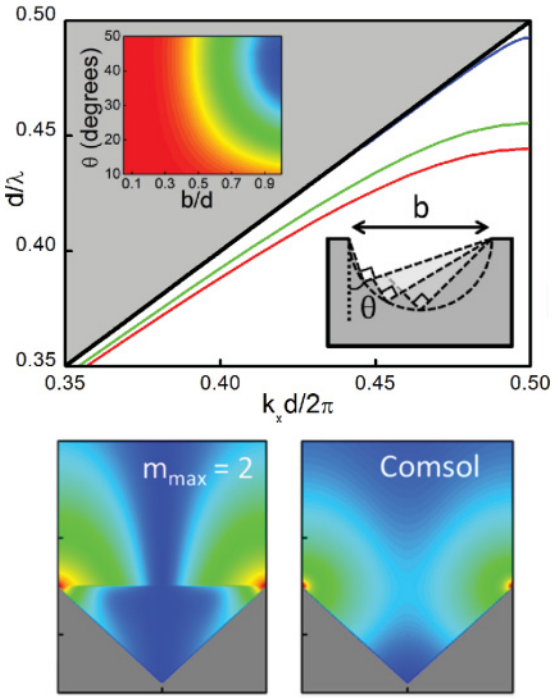


FIG. 4. (Color online) Upper panel: Spoof SPP dispersion relation for triangular grooves with $b = 0.7d$, and three different angles: 15° (blue), 30° (green), and 45° (red). The inset shows $d/\lambda$ at the band edge as a function of $b/d$ and $\theta$. The color scale ranges linearly from 0.42 (blue) to 0.5 (red). Note that these results have been compared with simulations and been found to be in a good agreement. Lower panel: $|E|$ at $k_x = \pi/d$ for a sawtooth surface with $b = d$ and $\theta = 45°$ calculated for $m_{\max} = 2$. The corresponding numerical field map is also shown. In both panels the color ranges linearly from blue (minimum) to red (maximum).

A schematic of this geometry is shown in the lower inset of the top panel of Fig. 4. Note that our description is limited to right-angled triangular dents. Thus, for fixed $b$, as $\theta$ increases the possible triangles that can be modeled by our theoretical approach trace out a semicircle. Moreover, by specifying a right-angled triangular groove, we reduce the number of geometric parameters defining the structure from 3 to 2. Note that in general there are now more than one set of parameters that specify a single triangular geometry.

The top panel of Fig. 4 renders the dispersion relation of the spoof plasmon modes supported by a periodic array of triangular dents of width $b = 0.7d$, and three different orientation angles, 15° (blue line), 30° (green line), and 45° (red line). As expected, increasing $\theta$ redshifts the dispersion relation, which departs further from the light line. This results from the fact that for a fixed groove width, larger orientation angles translate into an increase of the indentation vertical depth. Thus, for larger $\theta$, EM fields penetrate deeper into the corrugated PEC surface, which yields greater confinement of the spoof SPP modes.

The inset to Fig. 4 displays the normalized frequency evaluated at the band edge for a wide range of groove widths and orientation angles. Colors render $d/\lambda$ in a linear scale from 0.42 (blue) to 0.5 (red). The dents with small $b$ are very shallow for all $\theta$, and hence the spoof SPP dispersion relation lies close to the light line. For triangular grooves with higher $b$, the decrease of the normalized frequency with increasing $\theta$ is clearly visible. This indicates the binding of the spoof SPPs to the indentations associated with the effective deepening of the structure corrugation. Note that for all widths, $d/\lambda$ reaches its lowest value for $\theta = 45°$, as it is at this point that the triangular dent is at its deepest with respect to the PEC surface. Although it is not shown in Fig. 4, full field numerical calculations were also performed for triangular indentations and the results were found to be in a good agreement with our model. As in the case of slanted grooves, for larger $\theta$ the convergence is worse, but of a similar size to that shown in Fig. 3.

Finally, we explore triangular dents having $b = d$. In this limit, the PEC structure supporting spoof SPPs is no longer a planar interface decorated with indentations, but a completely triangular *sawtooth* surface. The inset of Fig. 4 shows that the spoof plasmon modes in this geometry are the most sensitive to changes in the orientation angle. We focus on the case $\theta = 45°$, which yields the lowest modal frequency ($d/\lambda \sim 0.42$ at the band edge) and hence the highest field confinement. The lower two panels of Fig. 4 depict $|E|$ evaluated at $k_x = \pi/d$ for a sawtooth surface with $b = d$ and $\theta = 45°$. Two calculations are shown: quasianalytical results for $m_{\max} = 2$, and COMSOL simulations. The former were obtained through the asymmetric sum of the electric field patterns that our approach yields for the two possible groove orientations ($\theta = \pm 45°$) that give rise to the geometry under consideration. For the $\theta = +45°$ ($-45°$) orientation, the left (right) groove wall in Fig. 4 corresponds to the original groove bottom before rotation. Despite the evident field discontinuity at the structure interface, Fig. 4 demonstrates that by including only 3 groove waveguide modes, our quasianalytical calculations reproduce the main features of the numerical field pattern. In agreement with simulations, our theory predicts that spoof SPPs in sawtooth surfaces lead to the strongest field enhancements at the upper corners of the structure corrugation. This is qualitatively different from what is observed in rectangular grooves, where the hot spots are located within the indentations decorating the PEC surface.

Let us stress that in this work we have modeled the metal permittivity using the PEC approximation. In this way, the geometries analyzed herein can be scaled in size, making possible the exploration of spoof SPPs in different frequency ranges: microwave, terahertz, or optical. In the latter case, the dielectric function of noble metals such as gold or silver acquires low values, departing from the PEC behavior. This enables EM fields to penetrate into the metal structure, leading to the emergence of conventional plasmonic phenomena in the system. These effects are omitted in this paper. The interplay between pure geometric and intrinsic dielectric effects in optical spoof plasmons is currently being explored as a means to improve the waveguiding performance of conventional plasmonic devices.[51]

## IV. CONCLUSIONS

In conclusion, we have developed a refined quasianalytical approach that allows the theoretical investigation of spoof

plasmon polaritons supported by a perfectly conducting surface decorated by a periodic array of slanted grooves. We have presented an approximate analytical expression that provides an insightful description of the dependence of the spoof plasmon dispersion relation on the groove orientation. Combining theory and simulations, a comprehensive study of the effect of the groove rotation in rectangular geometries has been performed. Finally, we have shown that our method can be applied to the analysis of the spoof plasmon modes sustained by triangular indentations and sawtooth surfaces.


## ACKNOWLEDGMENTS

We gratefully acknowledge financial support provided by the Engineering and Physical Sciences Research Council (EPSRC) and the Leverhulme Trust.


## APPENDIX

In this Appendix, we provide expressions for the evaluated overlap integrals and the form of these equations that leads to the dispersion relation given by Eq. (11). The overlap integrals from Eqs. (6), (8), (9), and (10) can be written as follows:

$$S_{mn} = \sqrt{\frac{2-\delta_{m0}}{ad}}\frac{iq_n^I\cos\theta}{q_n^{I^2}-\left(\frac{m\pi\cos\theta}{a}\right)^2}\left[\exp\left(-i\frac{a}{2}q_n^I\sec\theta\right)-(-1)^m\exp\left(i\frac{a}{2}q_n^I\sec\theta\right)\right], \tag{A1}$$

$$\epsilon_{mm'} = Y_{m'}^{II}\cos\theta q_{m'}^{II}\sin\theta\frac{\sqrt{(2-\delta_{m0})(2-\delta_{m'0})}}{a\sin\left(q_{m'}^{II}h\right)}\left\{\sin\left[q_{m'}^{II}\left(h+\frac{a}{2}\tan\theta\right)\right]-(-1)^{m+m'}\sin\left[q_{m'}^{II}\left(h-\frac{a}{2}\tan\theta\right)\right]\right\}$$
$$\times\frac{q_{m'}^{II^2}\sin^2\theta-\left(\frac{\pi\cos\theta}{a}\right)^2(m^2+m'^2)}{\left(q_{m'}^{II^2}\sin^2\theta-\left(\frac{\pi\cos\theta}{a}\right)^2(m+m')^2\right)\left(q_{m'}^{II^2}\sin^2\theta-\left(\frac{\pi\cos\theta}{a}\right)^2(m-m')^2\right)}, \tag{A2}$$

$$X_{nm'} = \sqrt{\frac{2-\delta_{m'0}}{4ad}}\frac{1}{\sin\left(q_{m'}^{II}h\right)}\left(\frac{e^{iq_{m'}^{II}h}\left(q_{m'}^{II}\sin\theta+q_n^I\right)}{\left(q_{m'}^{II}\sin\theta+q_n^I\right)^2-\left(\frac{m'\pi\cos\theta}{a}\right)^2}\left\{(-1)^{m'}\exp\left[-i\frac{a}{2}\left(q_n^I\sec\theta+q_{m'}^{II}\tan\theta\right)\right]\right.\right.$$
$$\left.-\exp\left[i\frac{a}{2}\left(q_n^I\sec\theta+q_{m'}^{II}\tan\theta\right)\right]\right\}+\frac{e^{-iq_{m'}^{II}h}\left(q_{m'}^{II}\sin\theta-q_n^I\right)}{\left(q_{m'}^{II}\sin\theta-q_n^I\right)^2-\left(\frac{m'\pi\cos\theta}{a}\right)^2}\left\{(-1)^{m'}\exp\left[-i\frac{a}{2}\left(q_n^I\sec\theta-q_{m'}^{II}\tan\theta\right)\right]\right.$$
$$\left.\left.-\exp\left[i\frac{a}{2}\left(q_n^I\sec\theta-q_{m'}^{II}\tan\theta\right)\right]\right\}\right), \tag{A3}$$

$$Z_{nm'} = \sqrt{\frac{2-\delta_{m'0}}{4ad}}\frac{-i\cos\theta Y_{m'}^{II}}{k_\omega\sin\left(q_{m'}^{II}h\right)}\left(\frac{m'\pi}{a}\right)^2\left(\frac{e^{iq_{m'}^{II}h}}{\left(q_{m'}^{II}\sin\theta+q_n^I\right)^2-\left(\frac{m'\pi\cos\theta}{a}\right)^2}\left\{(-1)^{m'}\exp\left[-i\frac{a}{2}\left(q_n^I\sec\theta+q_{m'}^{II}\tan\theta\right)\right]\right.\right.$$
$$\left.+\exp\left[i\frac{a}{2}\left(q_n^I\sec\theta+q_{m'}^{II}\tan\theta\right)\right]\right\}+\frac{e^{-iq_{m'}^{II}h}}{\left(q_{m'}^{II}\sin\theta-q_n^I\right)^2-\left(\frac{m'\pi\cos\theta}{a}\right)^2}\left\{(-1)^{m'}\exp\left[-i\frac{a}{2}\left(q_n^I\sec\theta-q_{m'}^{II}\tan\theta\right)\right]\right.$$
$$\left.\left.+\exp\left[i\frac{a}{2}\left(q_n^I\sec\theta-q_{m'}^{II}\tan\theta\right)\right]\right\}\right). \tag{A4}$$

Next, when calculating the analytic dispersion relation only the $m = n = 0$ modes are considered, under the assumption that $\lambda \gg d \gg a$, and Eq. (5) can be reduced to

$$G_{00}-\epsilon_{00} = Y_0^I S_{00}(\cos\theta X_{00}-\sin\theta Z_{00})-\epsilon_{00} = 0, \tag{A5}$$

where

$$Y_0^I = \frac{-ik_\omega}{\sqrt{k_x^2-k_\omega}},\quad S_{00} = \sqrt{\frac{a}{d}},\quad X_{00} = \sqrt{\frac{a}{d}}\sec\theta,$$
$$\epsilon_{00} = -i\cot(k_\omega h)\mathrm{sinc}[(k_\omega a/2)\tan\theta].$$

Note that $Z_{00} = 0$, as it is proportional to $m^2$. Thus, after some algebra, Eq. (11) is obtained.


[1] R. H. Ritchie, Phys. Rev. **106**, 874 (1957).

[2] S. A. Maier, *Plasmonics: Fundamentals and Applications* (Springer Verlag, New York, 2007).

[3] M. L. Brongersma and V. M. Shalaev, Science **328**, 440 (2010).

[4] V. Giannini, A. I. Fernández-Domínguez, Y. Sonnefraud, T. Roschuk, R. Fernández-García, and S. A. Maier, Small **6**, 2498 (2010).

[5] J. N. Anker, W. P. Hall, O. Lyandres, N. C. Shah, J. Zhao, and R. P. Van Duyne, Nature Mater. **7**, 442 (2008).

[6]G. Gobau, J. Appl. Phys. **21**, 1119 (1950).
[7]R. Ulrich and M. Tacke, Appl. Phys. Lett. **22**, 251 (1973).
[8]D. L. Mills and A. A. Maradudin, Phys. Rev. B **39**, 1569 (1989).
[9]J. B. Pendry, L. Martín-Moreno, and F. J. García-Vidal, Science **305**, 847 (2004).
[10]A. P. Hibbins, B. R. Evans, and J. R. Sambles, Science **308**, 670 (2005).
[11]C. R. Williams, S. R. Andrews, S. A. Maier, A. I. Fernández-Domínguez, L. Martín-Moreno, and F. J. García-Vidal, Nature Phot. **2**, 175 (2008).
[12]F. J. García-Vidal, L. Martín-Moreno, and J. B. Pendry, J. Opt. A: Pure Appl. Opt. **7**, S97 (2005).
[13]M. Qiu, Opt. Express **13**, 7583 (2005).
[14]F. J. García de Abajo and J. J. Saenz, Phys. Rev. Lett. **95**, 233901 (2005).
[15]A. P. Hibbins, E. Hendry, M. J. Lockyear, and J. R. Sambles, Opt. Express **16**, 20441 (2008).
[16]Q. Gan, Z. Fu, Y. J. Ding, and F. J. Bartoli, Phys. Rev. Lett. **100**, 256803 (2008).
[17]E. Hendry, A. P. Hibbins, and J. R. Sambles, Phys. Rev. B **78**, 235426 (2008).
[18]M. R. Gadsdon, I. R. Hooper, A. P. Hibbins, and J. R. Sambles, J. Opt. Soc. Am. B **26**, 1228 (2009).
[19]J. T. Shen, P. B. Catrysse, and S. Fan, Phys. Rev. Lett. **94**, 197401 (2005).
[20]Z. Ruan and M. Qiu, Appl. Phys. Lett. **90**, 201906 (2007).
[21]S. A. Maier, S. R. Andrews, L. Martín-Moreno, and F. J. García-Vidal, Phys. Rev. Lett. **97**, 176805 (2006).
[22]A. I. Fernández-Domínguez, E. Moreno, L. Martín-Moreno, and F. J. García-Vidal, Phys. Rev. B **79**, 233104 (2009).
[23]A. I. Fernández-Domínguez, E. Moreno, L. Martín-Moreno, and F. J. García-Vidal, Opt. Lett. **34**, 2063 (2009).
[24]M. Navarro-Cía, M. Beruete, S. Agrafiotis, F. Falcone, M. Sorolla, and S. A. Maier, Opt. Express **17**, 18184 (2009).
[25]D. Martín-Cano, M. Nesterov, A. I. Fernández-Domínguez, E. Moreno, L. Martín-Moreno, and F. J. García-Vidal, Opt. Express **18**, 754 (2010).
[26]D. Martin-Cano, O. Quevedo-Teruel, E. Moreno, L. Martín-Moreno, and F. J. García-Vidal, Opt. Lett. **36**, 4635 (2011).
[27]A. I. Fernández-Domínguez, C. R. Williams, L. Martín-Moreno, F. J. García-Vidal, S. R. Andrews, and S. A. Maier, Appl. Phys. Lett. **93**, 141109 (2008).
[28]W. Zhu, A. Agrawal, and A. Nahata, Opt. Express **16**, 6216 (2008).
[29]M. J. Lockyear, A. P. Hibbins, and J. R. Sambles, Phys. Rev. Lett. **102**, 073901 (2009).
[30]W. Zhao, O. M. Eldaiki, R. Yang, and Z. Lu, Opt. Express **18**, 21498 (2010).
[31]C. R. Williams, M. Misra, S. R. Andrews, S. A. Maier, S. Carretero-Palacios, S. G. Rodrigo, F. J. García-Vidal, and L. Martín-Moreno, Appl. Phys. Lett. **96**, 011101 (2010).
[32]G. Kumar, S. Pandey, A. Cui, and A. Nahata, New J. Phys. **13**, 033024 (2011).
[33]S.-H. Kim, T.-T. Kim, S. S. Oh, J.-E. Kim, H. Y. Park, and C.-S. Kee, Phys. Rev. B **83**, 165109 (2011).
[34]E. M. G. Brock, E. Hendry, and A. P. Hibbins, Appl. Phys. Lett. **99**, 051108 (2011).
[35]Y. G. Ma, L. Lan, S. M. Zhong, and C. K. Ong, Opt. Express **19**, 21189 (2011).
[36]Y. J. Zhou, Q. Jiang, and T. J. Cui, Appl. Phys. Lett. **99**, 111904 (2011).
[37]T. Jiang, L. Shen, J. Wu, T. Yang, Z. Ruan, and L. Ran, Appl. Phys. Lett. **99**, 261103 (2011).
[38]X.-R. Huang, R.-W. Peng, and R.-H. Fan, Phys. Rev. Lett. **105**, 243901 (2010).
[39]N. Yu, Q. J. Wang, M. A. Kats, J. A. Fan, S. P. Khanna, L. Li, A. G. Davies, E. H. Linfield, and F. Capasso, Nature Mater. **9**, 730 (2010).
[40]A. B. Khanikaev, S. H. Mousavi, G. Shvets, and Y. S. Kivshar, Phys. Rev. Lett. **105**, 126804 (2010).
[41]B. Wang, J. Jiang, and G. P. Nordin, Opt. Express **12**, 3313 (2004).
[42]B. Wang, J. Jiang, and G. P. Nordin, IEEE Photonics Technol. Lett. **17**, 1884 (2005).
[43]J. Schrauwen, F. Van Laere, D. Van Thourhout, and R. Baets, IEEE Photonics Technol. Lett. **19**, 816 (2007).
[44]T. Levola and P. Laakkonen, Opt. Express **15**, 2067 (2007).
[45]N. Bonod, E. Popov, L. Li, and B. Chernov, Opt. Express **15**, 11427 (2007).
[46]B. Munk, *Frequency Selective Surfaces: Theory and Design* (Wiley, New York, 2000).
[47]A. A. Maradudin, *Structured Surfaces as Optical Metamaterials* (Cambridge University Press, Cambridge, 2011).
[48]A. Mary, S. G. Rodrigo, F. J. García-Vidal, and L. Martín-Moreno, Phys. Rev. Lett. **101**, 103902 (2008).
[49]F. J. García-Vidal, L. Martín-Moreno, T. W. Ebbesen, and L. Kuipers, Rev. Mod. Phys. **82**, 729 (2010).
[50]A. I. Fernández-Domínguez, F. J. García-Vidal, and L. Martín-Moreno, Phys. Rev. B **76**, 235430 (2007).
[51]M. L. Nesterov, D. Martin-Cano, A. I. Fernández-Domínguez, E. Moreno, L. Martín-Moreno, and F. J. García-Vidal, Opt. Lett. **35**, 423 (2010).